Higher-order ionosphere perturbations in GPS time and frequency transfer

S. Pireaux, P. Defraigne, L. Wauters, N. Bergeot, Q. Baire and C. Bruyninx
Royal Observatory of Belgium, 3 Avenue Circulaire, 1180 Brussels, Belgium; Email: sophie.pireaux@oma.be

***Abstract*— In high precision geodetic time transfer (i.e. based on precise modeling of code and carrier phase GPS data), the so-called ionosphere-free combination of the code (P_3) and carrier phase (L_3) measurements, made on the two GPS frequencies, is used to remove the first-order ionosphere effect. In this paper, we quantify the impact of residual second- and third-order ionosphere perturbations on geodetic time and frequency transfer solutions, for both continental baselines and intercontinental baselines. All time transfer computations have been done using the ATOMIUM software, developed at the Royal Observatory of Belgium. In order to avoid contamination by some imperfect modeling of the second- and third-order ionosphere effects in the satellite clock products, only single-difference (Common-View) processing is used, based on both code and carrier phase measurements. The results are shown for weak and for strong solar activity, as well as for particular epochs of ionosphere storms.**

I. Introduction

GPS signals are now commonly used to perform precise Time and Frequency Transfer (TFT) between two stations equipped with GPS receivers and stable atomic clocks. TFT combining the GPS phase (L) and code (P) signals is very precise and enjoys a high frequency stability thanks to the phase measurement precision (uncertainty uA - measurement errors - of about 0.1ns and a resolution of 1 observation per 30 seconds). The main limitation being GPS code calibration errors (uncertainty uB of $\sim$ 5ns).

However, the GPS signal is perturbed by the ionosphere it crosses. This can be even more dramatic when the signal encounters some local ionosphere disturbances called Traveling Ionosphere Disturbances or during a ionosphere storm. Since the ionosphere perturbation is frequency-dependent, it is commonly removed by combining the signals measured in the two GPS frequencies, L_1 and L_2. The so-called ionosphere-free combination (L_3 and P_3) however removes the first-order perturbations only. The aim of our work is to study the impact of second- and third- order ionosphere effects on Time and Frequency Transfer.

The outline of the present paper is as follows. In Section II, we briefly describe how higher-order ionosphere delays come into play in the L_3P_3-analysis. In Section III, the relevance of the Total Electron Content of the ionosphere is recalled. In Section IV, first-, second- and third-order ionosphere delay implementations are detailed. In Section V, we show the results obtained in terms of estimated ionosphere delays and in terms of their impact on the estimated station clock solution in Common View mode, whether for continental or for intercontinental baselines. In Section VI, we illustrate the correlations between ionosphere perturbations in TFT and space weather activity. We conclude in Section VII with some perspectives.

II. TFT ionosphere-free analysis using ATOMIUM

The present study was carried out using the ATOMIUM Software [Defraigne et al. (2008)], developed at the Royal Observatory of Belgium to perform precise geodetic TFT via GPS measurements. Taking advantage of the dual frequency GPS signals, ATOMIUM forms the so-called ionosphere-free signal combination from which the first-order ionosphere effect, $I1$, proportional to the inverse of the square of the GPS signal frequency, is removed. The ionosphere-free combination, further corrected for the second- and third-order ionosphere effects, reads [Pireaux et al. (2009)]:

$$\begin{aligned}(P_3)_p^i &= \rho_p^i + c\Delta t_p + c\Delta\tau^i + zpd_p + \varepsilon_P \\ &\quad + (+2\cdot I2_3 - 3\cdot I3_3)_p^i \\ (L_3)_p^i &= \rho_p^i + c\Delta t_p + c\Delta\tau^i + zpd_p + N_p^i\lambda_3 + \varepsilon_L \\ &\quad + (-I2_3 + I3_3)_p^i\end{aligned} \tag{1}$$

As can be seen in Equation 1, for the ionosphere-free combination (labelled with subscript 3), second-order ionosphere delays ($I2$) impact twice more the code than the phase; while third order delays ($I3$) impact three times more the code than the phase. The signs of the contributions for phase and code are also opposite. Other parameters in these observation equations, aside the higher-order ionosphere effects ($I2$, $I3$) and the station clock synchronization error (Δt_p) on which we shall focus, are the geometric distance between satellite i and station p (ρ_p^i), the satellite clock error ($\Delta\tau^i$) for which we use a priori values from the IGS [IGS data and products (2009)], the zenith troposhere path delay (zpd_p), phase ambiguities (N_p^i) multiplied by the ionosphere-free combination wavelength (λ_3) and unmodeled multipath plus other noises (ϵ_P, ϵ_L). ATOMIUM works either in Precise Point Positioning (PPP) mode [Kouba & Heroux (2001)], that is zero differences, or in Common View (CV) mode, that is single differences between simultaneous observations of a GPS satellite by two stations. For this study, we used the Common View mode since it allows to get rid of higher-order ionosphere perturbations on satellite clocks, as the IGS products do not take those into account.

III. Total Electron Content of the ionosphere

The key to ionosphere perturbations is the Total Electron Content (TEC) of the Earth ionosphere, that is the integrated

978-1-4244-3510-4/09/$25.00 ©2009 IEEE

electron density inside a column cylindar of unit base area around a given radial direction from Earth to satellite altitude. It is measured in TECU with 1 TECU = 10^{16} $electron/m^2$. It is function of the latitude and longitude, of the time of the day, of the time of the year, and of some occasional events (such as space weather or earthquakes) influencing the ionosphere state.

Slant TEC (STEC) is measured along the satellite-receiver signal trajectory. STEC is taken at the Ionosphere Piercing Point (IPP). With the increasing solar activity in the coming years, we shall expect increasing GNSS ionosphere induced errors. Figure 1 illustrates the impact of an ionosphere storm on STEC. STEC is there computed for satellite 18 seen by GPS stations located at Brussels (BRUS), Onsala (ONSA) and Paris (OPMT) on the 11th of March 2007, a ionosphere-quiet day (Figure 1a). STEC is normally larger at local noon (as TEC is maximal at that time) and when satellite elevation is the smallest (at the beginning and at the end of each satellite arc), as the GPS signal then travels longer through the ionosphere. When the ionosphere is quiet, STEC curves nicely pile up. In case of an ionosphere storm such as in the evening of the 30th October 2003 (Figure 1b), STEC curves are perturbed and STEC reaches higher values. Also, as 2003 (Figure 1b) was closer to a solar maximum than 2007 (Figure 1a), STEC was globally higher in 2003.

IV. Ionosphere delays

At any order, ionosphere delays on GPS signals are proportional to STEC. The factor of proportionality of a given ionosphere order effect with STEC depends on a given frequency labelled k. For the first order [Bassiri & Hajj (1993)],

$$I1_k = \alpha 1_k \cdot STEC \tag{2}$$

it is zero for the well named ionosphere-free combination, while it is given by Equation 3 for the so-called geometry-free combination (labelled with subscript 4, it is the difference between codes or phases respectively, at the two GPS emitting frequencies):

$$\begin{aligned} \alpha 1_3 &= 0 \\ \alpha 1_4 &= -40.3 \left(\frac{1}{f_1^2} - \frac{1}{f_2^2} \right) \end{aligned} \tag{3}$$

In the present study, we computed STEC via ATOMIUM from the geometry-free combination, using the first-order ionosphere-perturbation term only (which accounts for up to 99.9% of total ionosphere perturbations) and the precise phase measurements which we aligned with the code (First and second terms in Equation 4) from references [Hernandez-Pajares et al. (2007)] and [Hernandez-Pajares et al. (2008)]. The STEC estimate is further corrected for the receiver and satellite $P_1 - P_2$ Differential Code Biais (DCBs) (Third term in Equation 4):

$$(STEC)_p^i = \frac{1}{\alpha 1_4} \begin{bmatrix} (L_4)_p^i \\ -\left\langle (L_4)_p^i - (P_4)_p^i \right\rangle_{\substack{arc\ without \\ cycle\ slips}} \\ -c \cdot DCB_p - c \cdot DCB^i \end{bmatrix} \tag{4}$$

We used the a priori information on DCBs from CODE IONEX files [CODE GIMs (2009)].

The STEC we obtained via ATOMIUM is then used to estimate higher-order ionosphere corrections. At second order, in addition to the actual STEC value, the magnitude and sign of the ionosphere contribution also depend on the satellite-receiver signal direction (named LOS for the Line Of Sight in the following) via the angle θ_{B-LOS}, and on the geomagnetic field amplitude B at Ionosphere Piercing Point (IPP) [Pireaux et al. (2009)]. Hence, we used the following expression [Hernandez-Pajares et al. (2007)] in the no-bending approximation

$$I2_k = \alpha 2_k \cdot B_{IPP} \cdot \cos\theta_{B-LOS} \cdot STEC \tag{5}$$

with the frequency factor for the ionosphere-free combination

$$\alpha 2_3 = -\frac{7517 \cdot c}{2 \cdot f_1 f_2 (f_1 + f_2)} \tag{6}$$

to correct each individual L_3, P_3 measurement. We computed the geomagnetic field at IPP using the accurate International Geomagnetic Reference (IGR) model [Tsyganenko (2005)], since this allows to reduce errors in $I2$ up to 60% with respect to a dipolar model [Hernandez-Pajares et al. (2007)].

The third-order effect can easily be computed from STEC [Fritsche et al. (2005)]:

$$I3_k = \alpha 3_k \cdot STEC \tag{7}$$

with the frequency factor for $L_3 P_3$

$$\alpha 3_3 = -\frac{2437 \cdot N_{\max} \cdot \eta}{3 \cdot f_1^2 \cdot f_2^2} \tag{8}$$

also being function of the electronic distribution in the ionosphere via a shape factor, η (taken as 0.66), and a peak electron density value, N_{max}, which characterize the electron densities in the different ionosphere sublayers [Brunner and Gu (1991)]. We selected them rather empirically, but owing to the weak impact of $I3$ (see Section V-B), it is sufficient.

V. Results

A. In terms of ionosphere delays

We now have a look at the results obtained via ATOMIUM, first in terms of computed ionosphere delays. We chose station Onsala as an example, on a quiet (11th March 2007), versus on a stormy day (30th October 2003). On the quiet day, the first-order ionosphere perturbations cause delays of the order of 20 nanoseconds (Figure 2a). There, each small concave curve that constitutes the graph follows the STEC corresponding to an observed satellite arc with the usual maximum of STEC at local noon. On the perturbed day, the impact of a storm is clearly seen with $I1$ on the second GPS frequency reaching up to about a hundred nanoseconds (Figure 2b).

Second-order ionosphere delays on the ionosphere-free phase are 3 to 4 orders of magnitude smaller than first-order delays, with about 8 picoseconds at maximum on the quiet day (Figure 3a). This doubles at the peak activity of the storm

on the perturbed day, reaching about 15 picoseconds (Figure 3b).

Third-order ionosphere delays in the ionosphere-free phase are yet one order of magnitude smaller than the second order. They reach 0.12 picoseconds at the maximum of the quiet day (Figure 4a); while about 1.5 picoseconds at the maximum of the ionosphere storm (Figure 4b).

B. In terms of the impact on estimated clock solutions

To understand the impact of higher-order ionosphere delays on geodetic precise TFT, we first take the example of the continental baseline Brussels-Onsala, on the perturbed day 30th October 2003. Figure 5 illustrates the effect of $I2$ on the ionosphere-free combination, as the difference between estimated CV station clock synchronization error, with or without second-order ionosphere corrections applied. The impact of the evening ionosphere storm is there clearly seen: about 10 picoseconds peak to peak. We recall that, in common view, it is the differential effect, between the two stations, of ionosphere perturbations that matters.

In fact, $I3$ lays within the GPS noise level, hence is negligible. $I2$ is thus the most relevant contribution for higher-order ionosphere perturbations. The offset of the time transfer curve is given by the code, on which the second-order differential ionosphere correction is applied twice (see Equation 1). Whereas $I2$ is applied once only on phases and with the opposite sign, that is for frequency transfer.

On intercontinental baselines, the second-order ionosphere perturbation during the Halloween storm of October 2003 is also clearly visible. Furthermore, on some intercontinental baselines (such as for the BRUS (Belgium)-NRC1 (Canada) link shown in Figure 6), the difference in STEC content for the two stations can lead to an important second-order ionosphere contribution to the clock solution, even without an ionosphere storm. Indeed, the maximum of STEC at the two stations is not reached at the same time of the day, owing to the stations very different longitudes. And this differential STEC can be important in case of a high base-TEC level such as exists around a solar maximum.

VI. Correlations Space Weather

We are now slowly exiting a minimum of solar activity to move on to next 24th solar maximum of the famous 11-year solar cycle. In the previous section, we emphasized the need for higher-order ionosphere corrections on GPS signals in precise time and frequency transfer. We now stress the need for space weather products, via examples of correlations between space weather and ionosphere perturbations in GPS TFT.

A. Solar events, geomagnetic storms and GPS signal perturbations

In Figure 7, we provide the computed STEC above station Onsala using ATOMIUM, together with the K-index measured at Wingst Observatory on Earth, and a list (read [Pireaux et al. (2009)] for more details) of the most powerful solar X-ray flares named M and X, from the 26th October

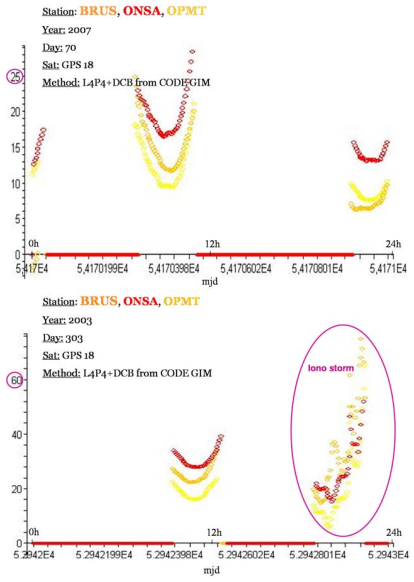

Fig. 1. STEC taken at Brussels (BRUS), Onsala (ONSA) and Paris (OPMT) GPS stations on an ionosphere-quiet day (Figure a, upper) or on a stormy day (Figure b, lower). 1 TECU= 10^{16} e^-/m^2.

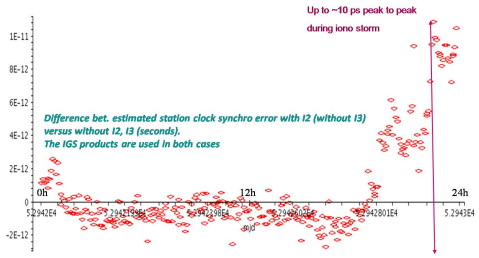

Fig. 5. Effect of taking second-order ionosphere effects, or not, into account in the L_3P_3 GPS measurements for the continental baseline Brussels (BRUS)-Onsala (ONSA) link, on the ionosphere-stormy day 30th October 2003. The difference is taken between two ATOMIUM estimated station clock solutions, both using IGS products.

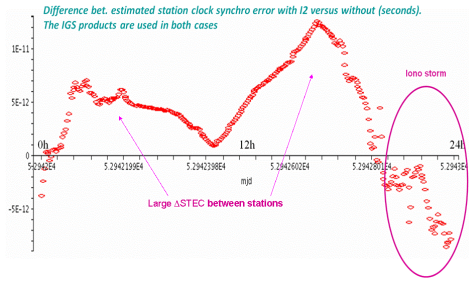

Fig. 6. Effect of taking second-order ionosphere effect, or not, into account in the L_3P_3 GPS measurements for the intercontinental baseline Brussels (BRUS)- Canada (NRC1) link, on the ionosphere-stormy day 30th October 2003. The difference is taken between two ATOMIUM estimated station clock solutions, both using IGS products.

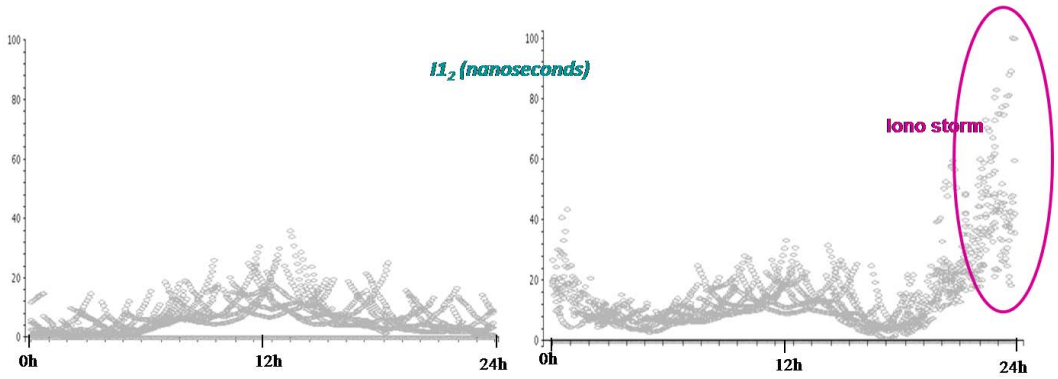

Fig. 2. First-order ionosphere delay in GPS frequency 2 ($I1_2$), for station Onsala on an ionosphere-quiet day, 11th March 2007 (Figure a, left), versus on an ionosphere-stormy day, 30th October 2003 (Figure b, right).

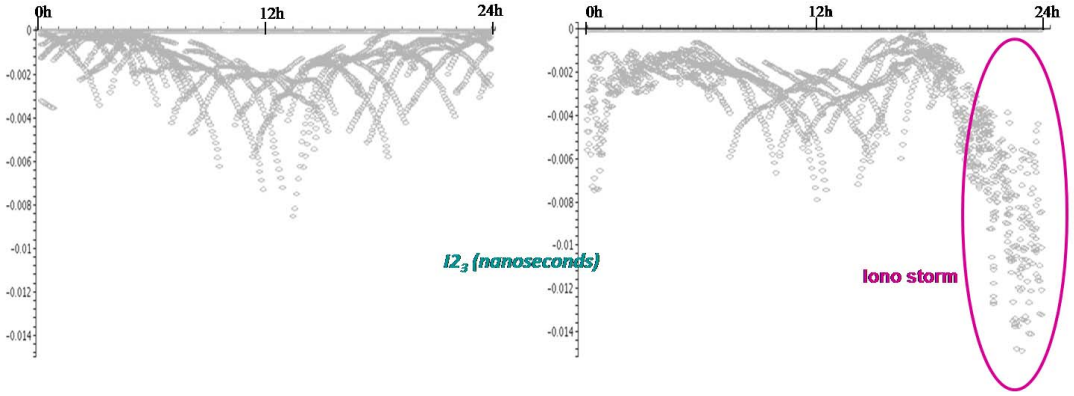

Fig. 3. Second-order ionosphere delay in GPS so-called ionosphere-free combination ($I2_3$), for station Onsala on an ionosphere-quiet day, 11th March 2007 (Figure a, left), versus on an ionosphere-stormy day, 30th October 2003 (Figure b, right).

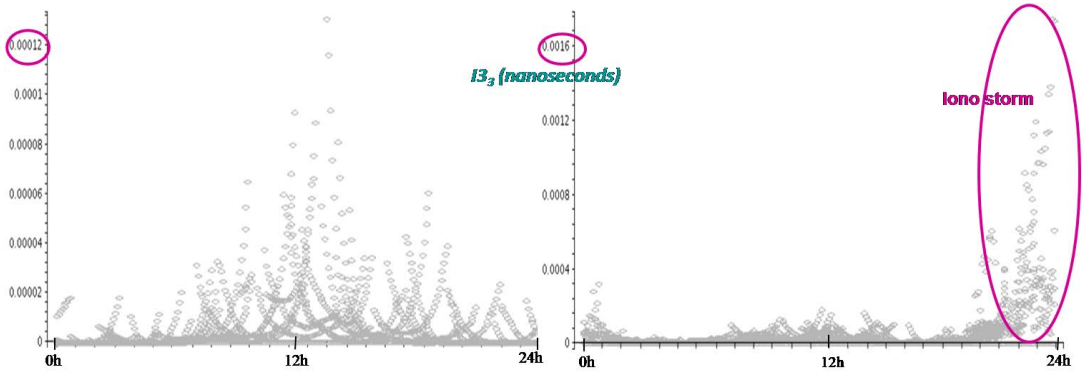

Fig. 4. Third-order ionosphere delay in GPS so-called ionosphere-free combination ($I3_3$), for station Onsala on an ionosphere-quiet day, 11th March 2007 (Figure a, left), versus on an ionosphere-stormy day, 30th October 2003 (Figure b, right).

to the 9th November 2003. Indeed, solar X-ray flares are often more frequent and stronger around maximums of the so-called 11-year solar cycle. Some flares may give rise to Coronal Mass Ejections (CMEs), those are ejections of plasma, carrying a magnetic field that might reach the Earth [Berghmans et al. (2005)]. If it occurs, it perturbs the Earth's magnetosphere and hence the Earth's ionosphere. The K-index quantifies disturbances in the horizontal component of the Earth's magnetic field, as observed with a magnetometer during a three-hour interval, with an integer in the range 0-9. The K-index reaches 5 and higher, in case of a geomagnetic storm. Figure 7 indicates how X flares accompanied by CMEs triggered some geomagnetic storms around the 30th October 2003.

The huge solar X-ray flare event X17.2 and its associated CME of October 28 2003, through the geomagnetic storm it triggered on the 29th October, is seen to be responsible for the abnormally high level of STEC at Onsala at early hours of the 30th October. This explains the correspondingly high first- and higher-order ionosphere perturbations computed in Figures 2b, 3b and 4b in the first hours of October 30, 2003. A small corresponding impact can be seen in the ATOMIUM clock solution, whether for continental (Figure 5) or for intercontinental baselines (Figure 6).

The major geomagnetic storm that occured in the evening of the 30th October, however, is most probably due to the solar X-ray flare event X10.1 and its associated CME of the 29th October. It lead to a very strong signature in the estimated STEC for Onsala in the evening of the 30th October (Figures 1b and 7); and hence in the first- and higher-order ionosphere perturbations on GPS signals (Figures 2, 3 and 4). The consequences can be seen in estimated Common View clock solutions computed with ATOMIUM, whether for continental (Figure 5) or for intercontinental baselines (Figure 6).

On the other side, the 11th March 2007 corresponds to quiet space weather conditions, without any M or X X-ray solar flare event (Figures 1a, 2a, 3a and 4a).

B. Stormy variations of the Earth magnetic field

We need to make some important remarks with respect to the results obtained with the second-order ionosphere corrections described in Section V. The IGR field model we used tracks usual longitudinal and latitudinal variations of the field, but not the sudden and important changes brought by an ionosphere storm. Hence, during a storm, real and local (interpolated) data are needed for the geomagnetic field at Ionosphere Piercing Point. Furthermore, in view of some real measurements of the geomagnetic field on the stormy day of the 30th October 2003, [Niemegk geomagnetic field Observations (2009)], we may not discard the possibility that the impact of second-order ionosphere perturbations on TFT during a storm might be higher than computed and might even reach the level of the nanosecond, since the geomagnetic field can be enhanced by a factor ~ 100. Consequently, until more realistic geomagnetic field values (such as interpolations at IPP from a grid of measurements) are available during a storm, one should not trust TFT computations during a storm.

However on intercontinental baselines, we have seen that when the base-TEC level is high, second-order ionosphere perturbations might be relevant to TFT (of the order of 10 picoseconds, Figure 6), aside a geomagnetic storm event. And then, fortunately, the IGR model for the geomagnetic field can be used.

VII. Conclusions

To conclude, the orders of magnitude of the estimated ionosphere delays, which are proportional to the Slant Total Electron Content (STEC) along the signal path in the ionosphere, can be summarized as follows.

First-order ionosphere delays on both GPS frequencies phase and code measurements are several tens of nanoseconds on a quiet day. They can reach about 100 nanoseconds on a stormy day.

Second-order delays on phases, which depend not only on STEC, but also on the Earth magnetic field at Ionosphere Piercing Point, are 3 to 4 orders of magnitude smaller than the first-order delays. They can reach around 15 picoseconds on a stormy day. However, the ionosphere storm impact on second-order delays might be under-estimated. Indeed, it was computed with the International Geomagnetic field Reference (IGR) model which does not contain the sudden and important variations of the true geomagnetic field during a geomagnetic storm.

Third-order ionosphere delays on phases are yet one order of magnitude smaller than second-order contributions.

Regarding the impact of those ionosphere delays on the Time and Frequency Transfer (TFT) in common view mode, the first order is completely removed in the ionosphere-free combination used in ATOMIUM.

The second order, in Common View, causes an effect up to 10 picoseconds in the clock solution on days of high ionosphere activity. This also traces the difference in time of the diurnal maximum TEC at the two stations on intercontinental baselines (since it is the differential ionosphere effect between stations that matters in Common View). The second-order ionosphere perturbations on TFT might even reach the level of the nanosecond during a storm, but the IGR model for the magnetic field is not sufficient in case of geomagnetic storm. Indeed, realistic values for the geomagnetic field at Ionosphere Piercing Point are then requested to compute second-order ionosphere delays.

Second-order ionosphere delays are applied once on phase (frequency transfer) and twice on code (time transfer). Under normal ionosphere conditions, they are smaller than present GPS calibration capabilities.

The third order is negligible in the so-called ionosphere-free TFT analysis.

Acknowledgment

This work has been supported by the Solar and Terrestrial Center

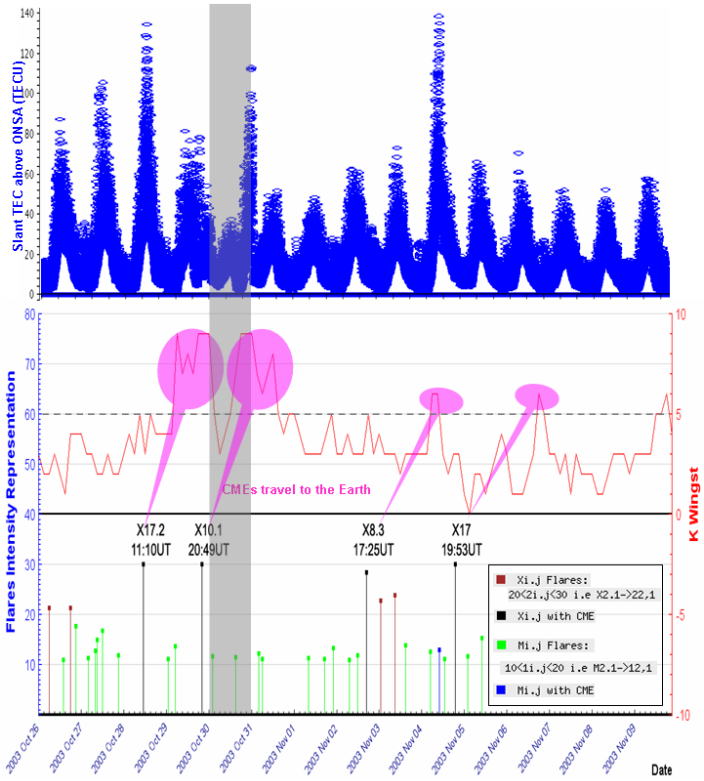

Fig. 7. Time series of the geomagnetic K index from Wingst Observatory, of the noticable solar events (X and M X-ray flares) and of STEC computed with the ATOMIUM software for the ONSA GPS station station Onsala, according to Equation 4, from 26th October to 9th November 2003. The notation used for solar X-ray flares is the following. Labels i and j are linked to the classification of flares. M flares are represented by a line peaking between 10 and 20 (e.g. M2.5 by a line from 0 to 12.5), while X flares are represented between 20 and 30, at their respective peak-intensity time. Note that X flares bigger than X9.9 saturate the scale and are represented by a line peaking at 30.

of Excellence [STCE (2009)]. The authors also acknowledge the IGS for their data and products [IGS data and products (2009)], the Solar Influences Data Analysis Center (SIDC) [SIDC (2009)] for their space weather weekly bulletin products and for their archives on solar events and related indexes, and the Niemegk Observatory for their geomagnetic field data [Niemegk geomagnetic field Observations (2009)].

REFERENCES

[Defraigne et al. (2008)] Defraigne, P., Guyennon, N., & Bruyninx, C., GPS Time and Frequency Transfer: PPP and Phase-Only Analysis, International Journal of Navigation and Observation, Vol. 2008, Article ID 175468, 2008.

[Kouba & Heroux (2001)] J. Kouba, & P. Heroux, GPS Precise Point Positionning using GPS orbit products, GPS solutions, 5, 12-28, 2001

[IGS data and products (2009)] IGS data and products. ftp://igscb.jpl.nasa.gov/

[Hernandez-Pajares et al. (2008)] Hernandez-Pajares, M. et al, Methods and other considerations to correct for higher-order ionospheric delay terms in GNSS, IGS workshop, Miami, USA, 2008, oral presentation.

[Bassiri & Hajj (1993)] Bassiri, S. , & Hajj, G. A., Higher-order ionospheric effects on the global positioning system observables and means of modeling them, Manuscripta Geodetica 18, 280-289,1993.

[Hernandez-Pajares et al. (2007)] Hernandez-Pajares, M., Juan, J. M., Sanz, J., & Oruz, R., Second-order ionospheric term in GPS: Implementation and impact on geodetic estimates, Journal of Geophysical Research, 112, B08417, 1-16, 2007.

[CODE GIMs (2009)] CODE Global Ionosphere Maps (GIMs). http://cmslive2.unibe.ch/unibe/philnat/aiub/content/e15/e59/e126/e440/e447/index_eng.html

[Tsyganenko (2005)] Tsyganenko, N.A., A set of FORTRAN subroutines for computations of the geomagnetic field in the Earth's magnetosphere, version of May 4, 2005, available on http://modelweb.gsfc.nasa.gov/magnetos/tsygan.html, as geopack-2005.doc and full fortran routines.

[Fritsche et al. (2005)] Fritsche, M., Dietrich, R., Knöfel, C., Rülke, A., & Vey, S., Impact of higher-order ionospheric terms on GPS estimates, Geophysical Research Letters 32, L23311, 1-5, Formula (14), 2005.

[Brunner and Gu (1991)] Brunner, F. K., & Gu, M., An improved model for the dual frequency ionospheric correction of GPS observations, Manuscripta Geodetica, 16, 205-214, 1991.

[Berghmans et al. (2005)] Berghmans, D., Van der Linden, R.A.M., Vanlommel, P., Warnant, R., Zhukov, A.N., Robbrecht, E., Clette, F., Podladchikova, O., Nicula, B., Hochedez, J.-F., Wauters, L., & Willems, S., Solar activity: nowcasting and forcasting at SIDC, Annales Geophysicae, 23(9), 3115-3128, 2005.

[Pireaux et al. (2009)] Pireaux, S., Defraigne, P., Wauters, L., Bergeot, N., Baire, Q., & Bruyninx, C., Influence of ionosphere perturbations in GPS time and frequency transfer, submited to the Special ASR Issue Entitled Recent Advances in Space Weather Monitoring, 2009.

[Niemegk geomagnetic field Observations (2009)] One-minute averages of Niemegk Observatory: View or download plots and ASCII listings of the Niemegk observatory data, http://www.gfz-potsdam.de/portal/-?$part=sec23&locale=en

[STCE (2009)] Solar and Terrestrial Center of Excellence (STCE), http://www.stce.be/index.php

[SIDC (2009)] Solar Influences Data Analysis Center (SIDC), http://sidc.oma.be/, hosted by the Royal Observatory of Belgium; SIDC space weather weekly bulletin: http://www.sidc.be/products/bul/index.php, bulletins 307 and 314.